



Adsorption of Phenol from Wastewater Using Microwave-Assisted Ag–Au Nanoparticle-Modified Mango Seed Shell-Activated Carbon

Idris Olanrewaju Okeowo^{1,2} · Ezekiel Olalekan Balogun^{1,2} · Ayodeji Joshua Ademola^{1,2} · Abass Olanrewaju Alade^{1,2,3} · Tinuade Jolaade Afolabi^{1,2} · Ebenezer Olujimi Dada¹ · Abolaji Grace Farombi^{2,4}

Received: 20 July 2019 / Revised: 4 January 2020 / Accepted: 18 January 2020 / Published online: 5 February 2020
© University of Tehran 2020

Abstract

Removal of phenol from simulated wastewater was investigated with silver–gold-nanoparticle-modified mango seed shell-activated carbon under batch experiment. The surface properties of the activated carbons were characterized using Fourier transform infrared spectroscopy (FTIR). Adsorption experiment was carried out at ambient temperature to study the effect of contact time, adsorbent dosage, and temperature on phenol adsorption. The equilibrium data were fitted to isotherm model, kinetic model, and intra-particle diffusion models. The maximum removal efficiencies increased from 55.5 to 94.55 and 71.4 to 98.1% for the unmodified and nano-modified activated carbon with increase concentration (50–250 mg/l). The correlation coefficient (R^2) Langmuir, Freundlich, and Temkin were 0.3554–0.4563 and 0.2813–0.3191, 0.9150–0.9596 for nanoparticle-modified activated carbon (NCAMSS), as well as 0.5853–0.6598, 0.8159–0.8642, and 0.8159–0.8642, for unmodified activated carbon (UCAMSS). The R^2 of the pseudo-first and pseudo-second orders as well as Elovich kinetic models were in the ranges 0.8661–0.9925, 0.8260–0.9942, and 0.6032–0.7505 for NCAMSS as well as 0.4846–0.6032, 0.9567–0.9929, and 0.8842–0.9786, for UCAMSS and modified activated carbon, respectively. The order of fitness/suitability of the models is pseudo-first order > Elovich > pseudo-second order. The intra-particle diffusion model showed that the rate-controlling step is influenced by pore diffusion and that boundary layer diffusion and the adsorption process is heterogeneous, exothermic, and spontaneous. It can be deduced that mango seed shell is a good precursor in the production of activated due to its high yield and good adsorption capacity and the modification of the activated carbon with nanoparticles increased the precursor adsorption properties.

Article Highlights

- Biosyntheses of silver/gold nanoparticles was successfully used to modify activated carbon developed from mango seed shell.
- The FTIR of the Mango seed shell AC and the nanoparticle-modified Mango seed shell AC indicated the presence of IR peak ranged from 729.5 to 3902.9 cm^{-1} and 717.8 to 3985.3 cm^{-1} , respectively.
- The adsorption results of both nanoparticle-modified and unmodified AC indicated removal efficiencies increased from 55.5 to 94.55% and 71.4 to 98.1%, respectively.

✉ Abass Olanrewaju Alade
aolade@lautech.edu.ng

¹ Department of Chemical Engineering, Ladoké Akintola University of Technology, Ogbomosho, Nigeria

² Bioenvironmental, Water and Engineering Research Group (BWERG), Ladoké Akintola University of Technology, Ogbomosho, Nigeria

³ Science and Engineering Research Group (SAERG), Ladoké Akintola University of Technology, Ogbomosho, Nigeria

⁴ Department of Science Laboratory Technology, Osun State Polytechnic, Iree, Nigeria

- Freundlich isotherm is suitable to fit the adsorption of phenol onto activated carbon produced from mango seed shell.
- The ΔH° values gotten were negative which varied from -8.8212 to -22.8643 KJ/mol for the unmodified AC and -3.694 KJ/mol to -31.402 KJ/mol for nanoparticle-modified ACs. This showed that the adsorption process of phenol was spontaneous and exothermic.

Keywords Activated carbon · *Cola nitida* · Mango shell · Silver–gold nanoparticle · Phenol

Introduction

Phenolic compounds are organic compounds characterised with hydroxyl group(s) directly bonded to one or more aromatic rings. The first member of the group is phenol, with the chemical formula of C_6H_6OH and all other members of the group are derivatives of phenol (Dixon and Paiva 1995). Phenolic compounds are introduced into the aquatic environment through various activities resulting from agricultural, domestic, industrial, and natural processes. High concentration of phenol and phenolic compounds in water bodies have been linked to the wastewater discharged from major manufacturing industries, domestic wastes, runoffs from agricultural fields particularly where phenol-based agrochemical have been extensively used and natural decomposition or degradation of organic matters present in the aquatic environment (Wallace 1996).

Phenolic compounds that undergo transformations in the water bodies usually produced other complex compounds, which are more harmful than the original compounds and tend to persist in the environment (Bruce et al. 1987; Kulkarni and Kaware 2013). These developments signifies that the presence of phenolic compounds in the aquatic environments is obnoxious, undesirable, and deleterious to human health as well as flora and fauna (Bruce et al. 1987; Tchounwou et al. 2014; Dieguez-Santana et al. 2016; Acosta et al. 2018; Tichapondwa et al. 2018). Thus, concerns have been raised to ameliorate the influence of wastewater containing phenol, which has to be removed, before being discharged into the environment and its eventual committal to aquatic environment (Acosta et al. 2018; Wang et al. 2018).

Various wastewater treatment techniques, such as extraction, polymerisation, electro-Fenton process, photocatalytic degradation, chemical and bacterial oxidation, and electrochemical and irradiation, have been used for the removal of phenol and phenol compounds from industrial wastewaters (Gupta et al. 2013). However, the reputation of these techniques has been relegated due to some challenges such as high cost, incomplete purification of phenol, formation of hazardous by-products, and relatively low efficiency.

Adsorption technique, which essentially involved the use of activated carbon (AC), has been favoured as efficient technique for the treatment of organic wastewaters (Alabi

et al. 2019). In addition, the adsorption process is preferable, because it is economical, easy to hand, and better efficiency, compared to other techniques (Zhong 2017). The activated carbon is characterised, generally, with various properties such as large surface area, improved surface chemistry, and pore volume, which are effective for the removal of organic pollutants, toxic heavy metal ions, and dyes from fluid stream (Bulgariu et al. 2011; Lin et al. 2013; Wang et al. 2018; Zbair et al. 2018a, b). Activated carbons can be produced from various types of synthetic materials, which may be sourced from the industries, or renewable raw materials, which are sourced from agricultural wastes, by-products, and residues (Zbair et al. 2017).

These materials (synthetic or renewable) are activated via chemical or physical activation, independently or combined (Zbair et al. 2017). Physical activation involves carbonization of the desired material at elevated temperature to produce char, which is devoid of volatile components (Williams and Reed 2003). Chemical activation involves impregnation of the desired material with acidic, basic, and salt chemicals (Williams and Reed 2003). This process may be followed by carbonization at elevated temperature or vice versa, and the use of microwave has been reported in recent time (Zbair et al. 2019). Common chemicals used for activation purposes are generally dehydrating agents that have the capacity to activate the functional adsorption sites, and increases the binding capacity of the desired material (Allen et al. 2008; Zbair et al. 2019). They include chloride salts (aluminium, ferric iron, magnesium, and zinc), hydroxide (calcium, potassium, and sodium), and mineral acids (phosphoric, sulphuric). We employed nanoparticles biosynthesized from waste biomass to improve the adsorptive capacity of the targeted precursor in this study. The search for cheap adsorbent has led to the increasing use of agricultural wastes in the preparation of adsorbent (Ahsaine et al. 2018) and mango seed shell is of no exception.

Mango (*Mangifera indica*) is a very common tropical fruits found widely in many towns and villages within the Savannah and Rain Forest regions of Nigeria. The edible parts of the mango fruit are the peel and the fibrous material, while the nuts are usually discarded as waste, thus making Mango seed shell a significant solid waste candidate during its season (Alencar et al. 2012). The indiscriminate disposal

of the Mango peels and shells, due to its high consumption, leads to littering of the environment and generation of odour when oxidized or fermented (Meireles et al. 2010).

Mango seed shell (MSS) has been used as precursor for the production of effective activated carbon (AC) used for removal of various types of dyes (Kumar and Kumaran 2005; Davila-Jimenez et al. 2009; Alencar et al. 2012). However, MSS has not been reported as raw or modified adsorbent for the removal of phenol-form aqueous medium. This work is aim at using AC produced from MSS, which was modified, further, with biosynthesized nanoparticle from *cola nitida* for the removal of phenol from aqueous medium. The study was conducted under batch and the data generated were evaluated with various adsorption study parameters to determinate the efficacies of the MSS as precursor for the production of activated carbon suitable for the removal of phenol from wastewater.

Methodology

Chemicals and Reagents

The agricultural precursor used for this study was discarded Mango seed shell. Major reagents such as BaCl_2 , AgNO_3 , and HAuCl_4 were supplied by major chemical companies such as Merck, Sigma-Aldrich, and BDH. All the reagents were all of analytical grade, and thus, they were used without further purification.

Preparation of Adsorbent

Sampling

The MSS was sourced from LAUTECH Teaching and Research Farm, LAUTECH, Ogbomoso, Nigeria. They were sorted to remove stones and dust after collection. They were then washed with mild detergents and rinsed with copious amount of distilled water to remove impurities on their surfaces (Bullut and Tez 2007), sun-dried for 3 days, and oven-dried at 105 °C to constant weight (Tossou et al. 2019). Thereafter, it was milled to uniform size to increase its surface area (Bullut and Tez 2007) before activation and carbonization.

Activation and Carbonization

The MSS precursor (10 g) was mixed with 300 ml of 0.1 M of BaCl_2 based on the impregnation ratio (1:0.033) in a beaker, for 24 h. The ratio is equivalent to 300 g of activant solution (assuming the density of the solution to be approximately 1 g/cm³) to 10 g of the precursor (Eq. 1). The mixture was subjected to microwave oven effect at 300 Hz for 30 min

and excess BaCl_2 was boiled-off to form a paste before being oven-dried at 110 °C for 2 h (Gumus and Okpeku 2015). The mixture was then washed with distilled water until pH 7, to remove all traces of the activant, since the BaCl_2 is water-soluble chloride, and then oven-dried to constant weight at a 105 °C:

$$\text{Impregnation ratio} = \frac{\text{Weight of activant}}{\text{Weight of precursor}}. \quad (1)$$

Crucibles with known weight were filled (about 70% capacity) with the BaCl_2 -activated mango seed shell (AMSS) precursor and then reweighed before being charged into muffle furnace at 500 °C and for 20 min, for carbonisation purpose. These values were achieved in the preliminary studies conducted (Okeowo et al. 2017). The carbonised AMSS (CAMSS) produced was cooled in a desiccator before being crushed, washed, and oven-dried to constant moisture content. It was then screened to the desired size of 200 µm and divided into two parts in which one part was taken for modification with biosynthesized nanoparticle, while the other parts was used as unmodified.

Modification of Carbonised Mango Seed Shell AC with Nanoparticle

Silver-gold nanoparticle (Ag–AuNPs) was synthesized from Kolanut (*Cola nitida*) plant as reported by Lateef et al. (2016) with slight modifications. The *Cola nitida* plant extract, which serves as the precursor for the nanoparticle synthesis, was obtained by dispersing *Cola nitida* plant powder (0.1 g) in 10 ml of distilled water and then heated in water bath at 60 °C for 1 h. The reddish-brown extract obtained was filtered through Whatman No. 1 and the filtrate was further centrifuged at 4000 rpm for 20 min to obtain supernatant without suspensions. The supernatants (1 ml) were mixed with 10 ml solution containing 1 mM (HAuCl_4) and 1 mM AgNO_3 in ratio 1:4, respectively. The mixture was subjected to effect of sunlight and the changes in its colour for the formation of nanoparticles (Ag–AuNPs) were monitored. The dried CAMSS (0.5 g) was soaked in 10 ml (0.5 mg/l) of freshly prepared Ag–AuNPs' solution in a conical flask and agitated at 200 rpm on a rotary shaker for 12 h (Olajire et al. 2017). The mixture was then charged into the microwave oven for 1 h at 400 Hz to facilitate effective thermal deposition of the nanoparticles onto the CAMSS. The Ag–Au nanoparticle-modified CAMSS (NCAMSS) was then filtered and dried at 110 °C to constant weight.

Adsorbent Characterization

Surface characteristics of the raw MSS, unmodified CAMSS (UCAMSS), and NCAMSS developed were conducted using

Fourier transform infrared spectroscopy (FTIR) analysis (Al-Qodah and Shawabkah 2009). Samples (0.1 g) of the materials, each, was mixed with 1 g of KBr (spectroscopy grade) in a mortar. Part of the mixed paste was introduced in a cell connected to a piston of a hydraulic pump giving a compression pressure of 15 kPa/cm². The solid disc developed from the compression, was heated in an oven at 105 °C for 4 h to prevent interference of water vapour or carbon dioxide molecules, before being transferred to the FTIR analyzer (PerkinElmer Spectrum 100 series FTIR Spectrometer, USA). Various functional groups present on the surface of the materials were analysed within the range of 400–4000 cm⁻¹. Corresponding peaks obtained showing the wavelengths of the different functional groups in the sample and the spectra observed were identified by comparing with the values in the library (Al-Qodah and Shawabkah 2009).

Adsorption Experiment

Preparation of Adsorbate

Simulated phenol wastewater was produced by preparing the desired concentration of phenol solution in a conical flask. This was done by preparing a phenol solution of 1000 mg/l concentration in a standard volumetric flask (Ashanendu et al. 2018). The stock solution was diluted to the desired concentrations of 50–250 mg/l for batch equilibrium studies (Amri et al. 2009).

Batch Adsorption Experiment

Batch adsorption of phenol from the wastewater was carried out using the UCAMSS and NCAMSS to evaluate their adsorption performance. The adsorptive capacity of the activated carbon produced was determined using the method adopted by Amri et al. (2009). The samples (0.1 g) were added to 100 ml of different initial concentrations of phenol in a conical flask and then agitated at 200 rpm. The aqueous samples were taken at pre-set time intervals and their residual concentrations were determined using UV/Vis spectrophotometer at 270 nm wavelength for phenol. The adsorption capacity was evaluated using Eq. 2, while Eq. 3 determined the percentage removal or removal efficiency:

$$\text{Adsorption capacity} = \frac{(C_0 - C_e) \times V}{M}, \quad (2)$$

$$\text{Removal(\%)} = \frac{C_0 - C_e}{C_0}, \quad (3)$$

where C_0 (mg/l) is the initial concentration of phenol in contact with adsorbent, C_e (mg/g) is the final concentration of phenol after the batch adsorption procedure at any time t ,

M (g) is the mass of adsorbent, and V is the volume (l) of the aqueous.

Adsorption Isotherm Studies

The equilibrium adsorption isotherm of phenol removal by the adsorbent produced was considered as important in the design of adsorption system. The adsorbent samples (0.1 g) was placed in a 250 ml conical flask containing 100 ml of phenol solution of different initial known concentration. The agitation speed was kept constant at 200 rpm for each run to ensure equal mixing and reach equilibrium at a given time period. The content was filtered using filter paper and the supernatant solution in each flask was analysed using UV/Vis spectrophotometer. The adsorption data were fitted to well-known isotherm models such as Langmuir, Freundlich, and Temkin. Their constants were evaluated from the plots developed based on the liner form of their Eqs. (4–6) (Freundlich 1906; Langmuir 1916). The Langmuir isotherm constants, b and q_{\max} , were determined from the plot of $1/q_e$ versus $1/C_e$. The Freundlich isotherm constants, K_f and n^{-1} , were determined from the plot of $\log q_e$ versus $\log C_e$, while the Temkin isotherm constants A and B were determined from the plot of q_e versus $\ln C_e$:

$$C_e/q_e = C_e/q_m + 1/q_m K_L, \quad (4)$$

$$\ln q_e = \ln K_f + \frac{1}{n} \ln C_e, \quad (5)$$

$$q_e = B \ln A + B \ln C_e, \quad (6)$$

where q_e is amount of adsorbate absorbed at equilibrium (mg/g), q_{\max} is maximum adsorption capacity (mg/g), b is Langmuir equilibrium constant (l/mg), C_e is equilibrium phenol concentration in the solution (mg/l), K_f is Freundlich constant ((mg/g) (l/mg)^{1/n}), $1/n$ is Freundlich exponent (dimensionless), A is the Temkin isotherm constant (l/g), and B is heat of sorption (J/mol), respectively.

Batch Kinetics Studies

The adsorption kinetics of phenol on adsorbent was investigated using pseudo-first order, pseudo-second order, and Elovich kinetic models (Eqs. 7–9). The plot of $\ln(q_e - q_t)$ against t gave a slope of K_1 and an intercept of q_e , linear plot of t/q_t against t gave $1/q_e$ as the slope and $1/K_2 q_e^2$ as the intercept (Alabi et al. 2019), and plot of q_t against $\ln t$ gave a linear slope of $(1/\beta)$ and an intercept of $1/\beta \ln(\alpha\beta)$. All the evaluated parameters were used to predict the behaviour of the adsorption process:

$$\ln(q_e - q_e) = \ln q_e - K_1 t, \quad (7)$$

$$\frac{t}{q_t} = \frac{1}{K_2 q_e^2} + t/q_e, \quad (8)$$

$$q_t = \frac{1}{\beta} \ln(\alpha\beta) + \frac{1}{\beta} \ln t, \quad (9)$$

where q_e and q_t (mg/g) are the amounts of adsorbate adsorbed at equilibrium and any time t (min) respectively, K_1 (min^{-1}) is the adsorption rate constant, and K_2 (g/mg h) is the rate of second-order adsorption, Where α is the initial adsorption rate ($\text{mg g}^{-1} \text{min}$) and β is related to the extent of surface coverage and the activation energy for chemisorption (g mg).

Adsorption Mechanism

The intra-particle diffusion rate model shows that the rate-limiting step is the transport of the solute from the bulk of the solution to the adsorbent pores through intra-particles process. Various adsorption studies indicate that solute uptake varies almost proportionally with $t^{1/2}$ rather than with the contact time, t (Ejikeme et al. 2014). The model is expressed in Eq. 10 and plot of q_t versus $t^{1/2}$ gave slope of K_{id} and intercept of C (mg/g). Value of C gives the idea about the thickness of boundary layer and it has been suggested that the magnitudes of C values is directly related to the surface sorption in the rate-controlling step (Ejikeme et al. 2014):

$$q_t = K_{id}t^{1/2} + C, \quad (10)$$

where K_{id} is the intra-particle diffusion rate constant ($\text{mg/g min}^{1/2}$) and C is the intercept.

Adsorption Thermodynamic

Thermodynamic properties of adsorption process depict the level of spontaneity in the process as indicated by the Gibbs free energy change, ΔG° (Dejene et al. 2016). The energy (ΔH°) and entropy (ΔS°) changes are evaluated, usually, to determine the Gibbs free energy of the process. The volume of phenol solution (100 mg/l), agitation speed (200 rpm), and dosages (0.1 g) of the adsorbents produced were kept constant, while the time and temperature were varied from 10 to 50 and 35 to 60 °C, respectively. The mixture after agitation was filtered and the supernatant was analysed using UV/Vis spectrophotometer. The free energy equation that factors the adsorption equilibrium constant (K_a) (Eq. 11) and the differential form (Eq. 12) that relates ΔG° and K_a , were used to facilitate the evaluation of ΔH° and ΔS° which were determined from the slope and intercept of the plot of ΔG° versus temperature, T (Eq. 13) (Krishnaveni and Renugadevi 2012):

$$-RT \ln K_a = \Delta G^\circ, \quad (11)$$

$$\frac{d \ln K_a}{dT} = \frac{\Delta H^\circ}{RT^2}, \quad (12)$$

$$\Delta G^\circ = \Delta H^\circ - T\Delta S, \quad (13)$$

where ΔG° (J/mol) is the standard free energy change, R (8.314 J/mol K) is the universal gas constant, and T (K) is absolute temperature.

Results and Discussion

Adsorbent Characterization

The FTIR revealed the extent of reduction, appearance, disappearance, or broadening of the peaks on the surfaces of the adsorbent developed after the carbonization and impregnation with AgNPs (Olajire et al. 2017). The presence of these functional groups on the adsorbents was responsible for preferences of different adsorbate adsorption from aqueous medium (Rai et al. 2015). The FTIR characterisation (Fig. 1a–c) indicated the presence of IR peak in the ranged 729.5–3902.9 cm^{-1} and the peak height in the ranged 38.2–39.8 cm for the raw MSS. The IR peak for UCAMSS ranged from 717.8 to 3985.3 cm^{-1} and the peak height was from 14.3 to 17.8 cm, while for the NCAMSS, the peak ranged from 725.8 to 3987.1 cm^{-1} and the peak height ranges from 4.5 to 12.1 cm (Fig. 1c). There was the appearance of the $\text{C}\equiv\text{C}$ at peak of 2191.4 cm^{-1} after the carbonization of the mango seed shell. There were changes in the functional groups of both samples. Upon surface modification, there are appearances of some additional peaks at 3568.7 cm^{-1} Ag–Au nanoparticles-modified AC that can be attributed to stretching vibration of OH. Prominent peaks identified on the surface of the NCAMSS includes 2539.3–2777.6 cm^{-1} regions, which is attributed to O–H stretch, while those identified at 3683.5 are attributed to O–H bending. The peaks are observed at 11,787.3 cm^{-1} denotes the presence of $\text{C}=\text{O}$ extending vibrations that is attributed to keto-carbonyl (1740 cm^{-1}), while the $\text{C}=\text{C}$ stretch may be attributed of aromatic rings that may be derivative of the mango seed shell (Bouchelta et al. 2008; Zbair et al. 2018b).

Batch Equilibrium Studies

Effect of Contact Time

The effect of contact time on adsorption of phenol onto prepared NCAMSS and UCAMSS (Fig. 2a, b) revealed that the uptake of phenol was rapid at the initial stage of

the contact time for all the concentrations (Srivastava et al. 2006). The maximum adsorption capacity (q_e) for 50 mg/l was 7 mg/g and 10 mg/g, while for 200 mg/l, the values were 20 mg/g and 30 mg/g for UCAMSS and NCAMSS, respectively. This is because all the active sites on the adsorbent are vacant at the beginning of the adsorption process. The percentage removal (Fig. 3a, b) followed similar trend. The removal efficiency for 50 mg/l was 55%

and 75% while for 200 mg/l, the values were 70% and 90% for UCAMSS and NCAMSS, respectively. The adsorption capacity and percentage removal of the NCAMSS were higher compared to the UCAMSS (Figs. 2a, b, 3a, b) respectively, for all the concentrations considered. It may be suggested that the interaction that exists between phenol and Ag nanoparticles influenced the adsorption process, besides Olajire et al. (2017) noted that Ag (1)

Fig. 1 **a** FTIR spectra of raw mango seed shell. **b** FTIR spectra of activated mango seed shell. **c** FTIR spectra of Ag–Au nanoparticle-modified activated carbon

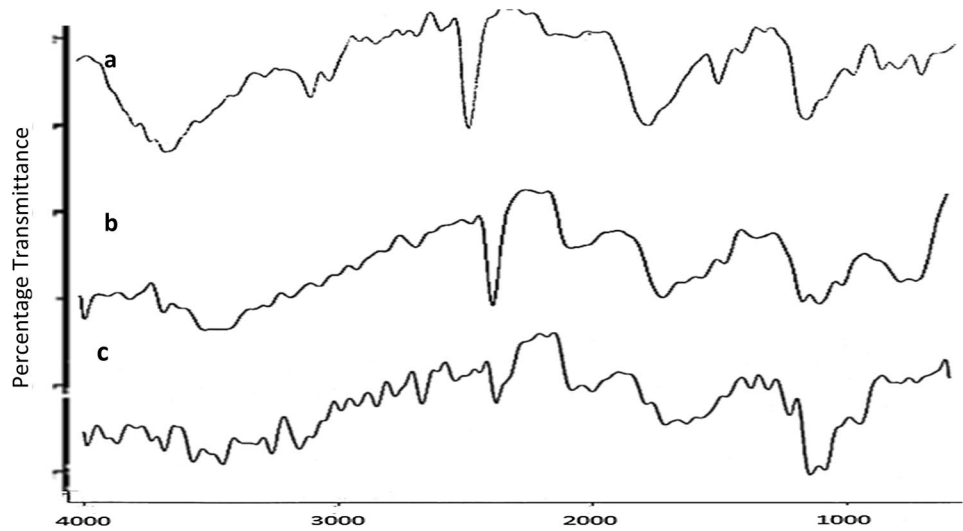


Fig. 2 Effect of contact time on adsorption of **a** 50 mg/l and **b** 200 mg/l of phenol

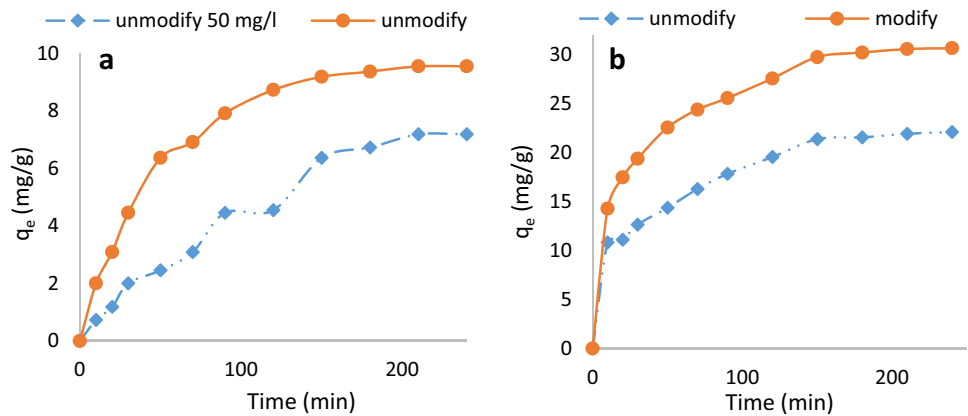
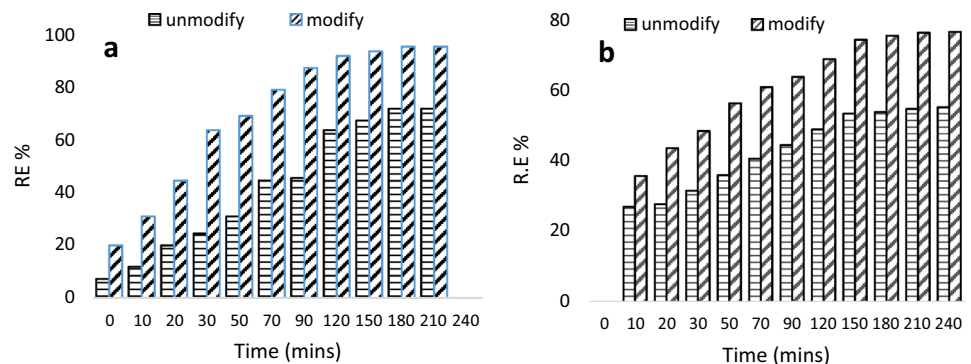


Fig. 3 Effect of time on percentage removal of **a** 50 mg/l and **b** 200 mg/l of phenol



ion, which is a weak Lewis acid, provides additional site in adsorption process.

Effect of Dosage

The adsorption study for adsorbent doses (0.1–0.5 g) (Fig. 4a, b) showed that the adsorption capacity increased from 27.7 to 47.27, and 35.7 to 49.3 mg/g, for both UCAMSS and NCAMSS. While their removal efficiencies increased from 55.5 to 94.55 and 71.4 to 98.1%, respectively. This can be linked, directly, to the availability of increasing adsorption sites with increasing amount of adsorbent, because, at higher adsorbent dose, there are not

enough phenol in the solution to occupy the active sites, and hence, the adsorption tends to become constant (Simhaet al. 2016). It was also discovered that the adsorption capacity and removal efficiency of the NCAMSS dosage were higher compared to the UCAMSS dosage (Fig. 4a, b).

Effect of Temperature

The three temperatures used for this study were 35 °C, 45 °C, and 60 °C, and their impact on adsorption capacity and removal efficiencies increased as the time increased from 10 to 50 min (Figs. 5a–c, 6a–c), respectively. The nanoparticle-modified AC have the higher adsorption rate and

Fig. 4 Effect of dosage on **a** adsorption capacity and **b** removal efficiency of nanoparticle-modified and unmodified mango seed shell-activated carbon

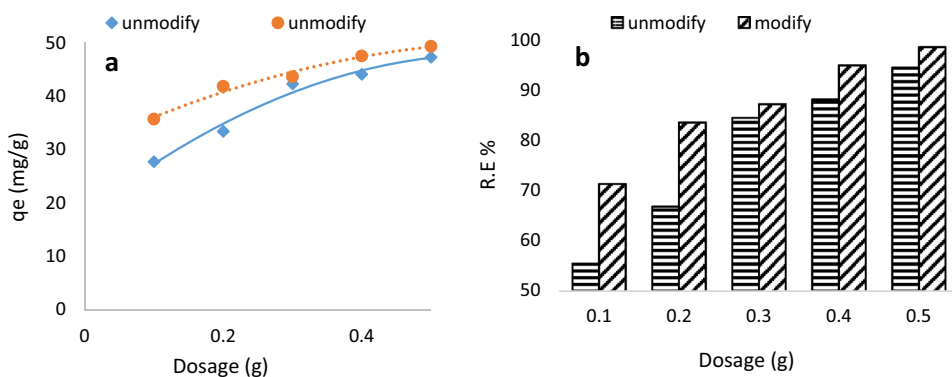


Fig. 5 Plot of q_e against time for **a** 35 °C, **b** 45 °C, and **c** 60 °C

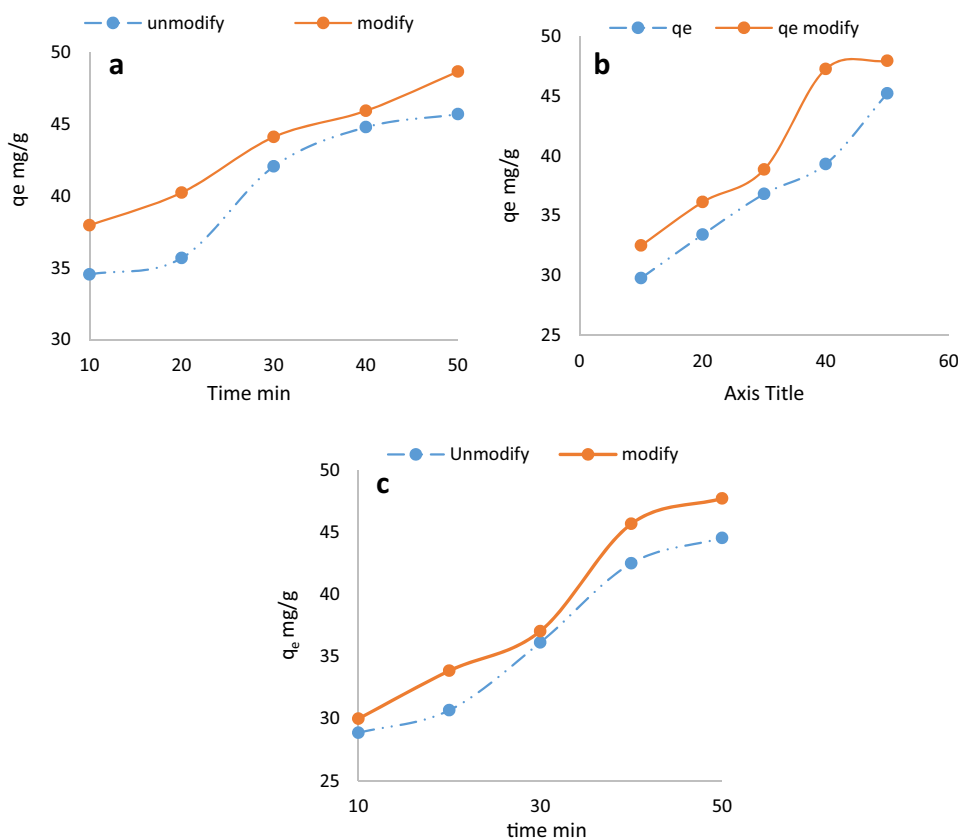
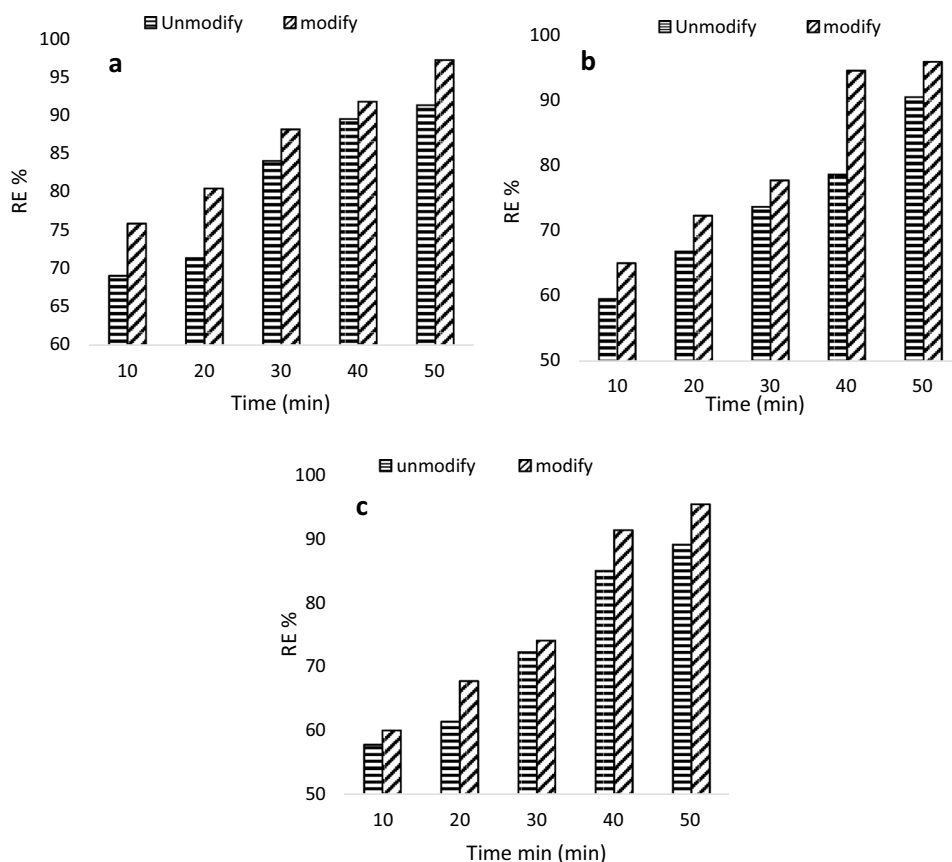


Fig. 6 Plot of R.E. against time for **a** 35 °C, **b** 45 °C, and **c** 60 °C



removal efficiency than the unmodified ones at the selected temperatures. The maximum q_e obtained for NCAMSS at 35, 45, and 60 °C were 48.63, 47.95, and 47.72 mg/g, respectively, while 45.68, 45.23, and 44.55 mg/g was obtained as maximum q_e for UCAMSS at 35, 45, and 60 °C, respectively. The maximum removal efficiency obtained for NCAMSS and UCAMSS at 35, 45, and 60 °C, were 97.27, 95.90, and 95.45% as well as 91.36, 90.45, and 89.10%, respectively. The adsorption capacity and removal efficiency decrease, as the temperature increases, and this means that the adsorption for phenol with the activated carbons is exothermic, and the lower temperature is favourable for adsorption of phenol (Zhang 2013). Studies reported by Varghese et al. (2004),

Shirzad-Siboni et al. (2013), Akpen et al. (2016), Olufemi and Otolorin (2017), and Fegousse et al. (2019) are with the same assertion that increase in temperature decreases the rate of adsorption (Table 1), though the findings of Tossou et al. (2019) were on the contradictory contrary converse.

Adsorption Isotherm

The plot of C_e/q_e versus q_e (Fig. 7a, b) based on linear method was used to determine the Langmuir parameters for the adsorption of phenol unto the unmodified and nanoparticle-modified mango seed shell-activated carbon. The Langmuir constants were evaluated from the slope $\frac{1}{q_m}$ and inter-

Table 1 Studies indicating the effect of temperature on increase in adsorption capacity

Material	Adsorbate	Temp trend	References
Water hyacinth	Phenol	Decreases	Varghese et al. (2004)
Activated Red mud	Phenol	Decreases	Shirzad-Siboni et al. (2013)
Mango seed endocarp-activated carbon	Dye	Decreases	Akpen et al. (2016)
Mango seed shell and mango seed shell-activated carbon	Crude oil	Decreases	Olufemi and Otolorin (2017)
Banana peel and cactus-activated carbon	Phenol	Increases	Tossou et al. (2019)
Pineapple bark	Dye	Decreases	Fegousse et al. (2019)
Mango seed shell-activated carbon and modified AC	Phenol	Decreases	This work

cept $\frac{1}{q_m K_L}$ (Tables 2, 3). The correlation coefficients (R^2) obtained for the NCAMSS (0.3554–0.4563) and UCAMSS (0.2813–0.3191) are essentially low (Tables 2), though those of NCAMSS were higher than UCAMSS, suggesting that

the adsorption on the surface of the adsorbents are not monolayer (Zbair et al. 2019). The K_L (l/mg), equilibrium constant, for NCAMSS and UCAMSS were in the range 0.0034–0.0073 l/mg and 0.0246–0.0502 l/mg. The K_L values are related to energy of distribution that depicts the affinity

Fig. 7 Plot of C_e/q_e against C_e for the adsorption of phenol on **a** unmodified and **b** nanoparticle-modified AC

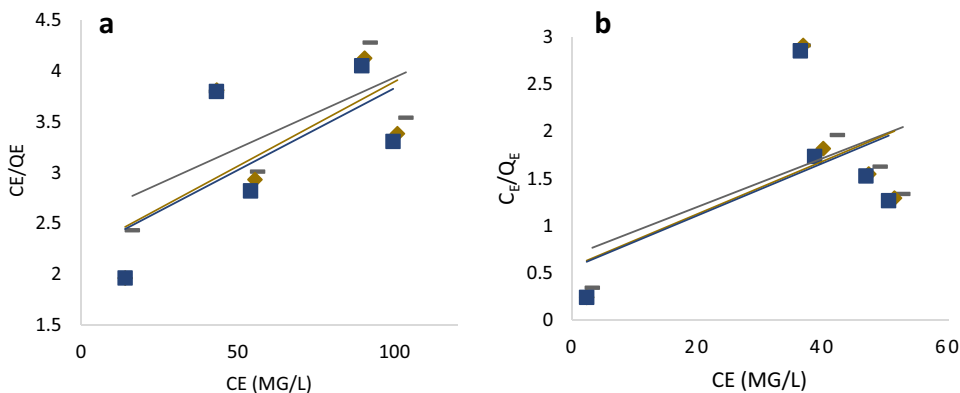


Table 2 Constants of Langmuir, Freundlich, and Temkin isotherm models for the adsorption of phenol on (a) unmodified and (b) nanoparticle-modified AC

Isotherm	Time (min)							
	Nano-modified activated carbon				Unmodified activated carbon			
	150	180	210	240	150	180	210	240
Langmuir								
Q_m	99.01	71.94	59.880	62.112	44.843	38.610	35.714	35.971
K_L	0.0034	0.0055	0.0075	0.0073	0.0246	0.0379	0.0495	0.0502
R_L	1.2029	0.7854	0.7276	0.7338	0.4484	0.3453	0.2879	0.2851
R^2	0.3554	0.4863	0.4846	0.4563	0.2813	0.2987	0.3202	0.3193
Freundlich								
K_F	2.3588	1.7278	1.2331	1.2930	0.2998	0.2539	0.1491	0.1478
$1/n$	0.8641	0.8055	0.7471	0.7607	0.6449	0.6428	0.5894	0.5911
n	1.1573	1.2415	1.3385	1.3146	1.5506	1.5556	1.6966	1.6918
R^2	0.9596	0.9473	0.9201	0.9150	0.6598	0.607	0.5798	0.5853
Temkin								
A	15.182	13.301	11.966	12.081	6.4308	5.9632	4.7167	4.6413
B	0.0748	0.0778	0.0800	0.0783	0.0694	0.0657	0.0713	0.0709
R^2	0.8642	0.8740	0.8604	0.8159	0.5321	0.4699	0.4516	0.4565

Table 3 Comparison of some adsorbents used for removal of phenol from aqueous solution

Adsorbent	n	Q_L	R_L	References
Unmodified mango seed shell AC	1.5506–1.6918	35.971–44.843	0.2851–0.4484	This study
Nano-modified mango seed shell AC	1.1573–1.3385	–99.01 to 62.11	0.7276–1.2029	This study
Organically modified manganite	NA	52.19	0.084	Ge et al. (2019)
Modified Rhassoul (clay)	NA	25	0.022	Hamdaoui et al. (2018)
Avocado kernel seed-activated carbon	4.73	0.215	9.4×10^{-5}	Dejene et al. (2016)
Kolanut shell-based-activated carbon	8.476	6.22	0.23	Lekene et al. (2015)
Luffa cylindrical fibres	1.8972	9.251	NA	Abdelwahab and Amin (2013)

NA not available

between the solute and adsorbent under investigation (Das et al. 2014). Specifically, the ranges of Q_m obtained are higher than those obtained for other adsorbents derived for manganite, clay, as well as avocado kernel seed, kolanut shell, and *Luffa cylindrica* fiber (Table 3). Similarly, the ranged of the R_L for our present study are higher than those obtained for the listed materials (Figs. 8, 9).

The essential characteristics of Langmuir isotherm can be explained in terms of a dimensionless constant, separation factor (R_L). The value of R_L , a positive number ($0 < R_L < 1$), signifies the feasibility of the adsorption process. The values of R_L for both the UCAMSS (0.2851–0.4484) and NCAMSS (0.7338–1.2029) activated are generally within the range, except for $R_L = 1.2029$, which is slightly above 1 (Table 3). The trend of favourability decreased with time and this suggests that lesser time favours the adsorption of phenol onto the mango-based adsorbent developed. This is another distinct property exhibited in this study. The ranges of R_L obtained in this study compared well with other R_L reported for other adsorbents developed from clay, seed shells, and biomass (Table 3).

The Freundlich parameters (n and K_F) and the R^2 were evaluated (Table 2). The Freundlich exponent, n , for the adsorption of adsorbate gave an indication on the favourability of adsorption. It is generally stated that the values of n in the range 2–10 represent ‘good’, 1–2 represents ‘moderately

good’, and less than 1 represents ‘poor’ adsorption characteristics. The values of ‘ n ’ obtained for the NCAMSS (1.1573–1.3146) and UCAMSS (1.5506–1.6918) can be rated as moderately good (Table 2). The large value of the R^2 (0.9150–0.9596 and 0.5853–0.6598) of Freundlich isotherm, compared to the Langmuir model, indicated that the Freundlich isotherm model fits the adsorption of phenol onto NCAMSS and UCAMSS better than Langmuir isotherm. It may further denoted multilayer nature of the adsorbent developed (Maet al. 2013). It was discovered that both the adsorption intensity K_F and the R^2 of the NCAMSS are higher than the UCAMSS, indicating that the nanoparticle used for the modification of the CAMSS has contributed to the properties of the adsorbent developed (Olajire et al. 2017).

The Temkin isotherm equilibrium-binding constant (α) (l/mg) for the NCAMSS (12.081–15.182 l/mg) and UCAMSS (4.6418–6.4308 l/mg) decreased as the contact time increased. The constant β , which is related to the heat of adsorption, did not display any clear relationship for the NCAMSS (0.0748–0.0800) and UCAMSS (0.0694–0.0713), although these values dropped from 0.0800 to 0.0783 and 0, 0713 to 0.0709, at the 240th min of the adsorption. High binding constant at lower time displayed the fact that lower time is needed for the adsorption process and this further indicated the economic importance

Fig. 8 Plot of $\log q_e$ against $\log C_e$ for the adsorption of phenol on **a** unmodified and **b** nanoparticle-modified AC

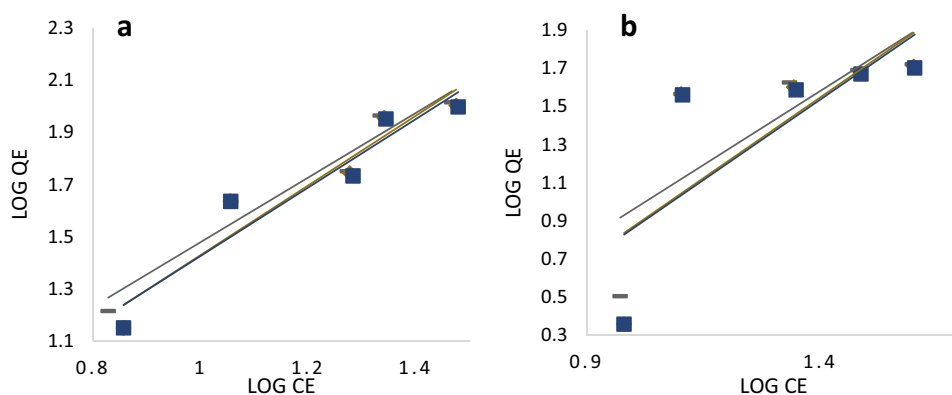
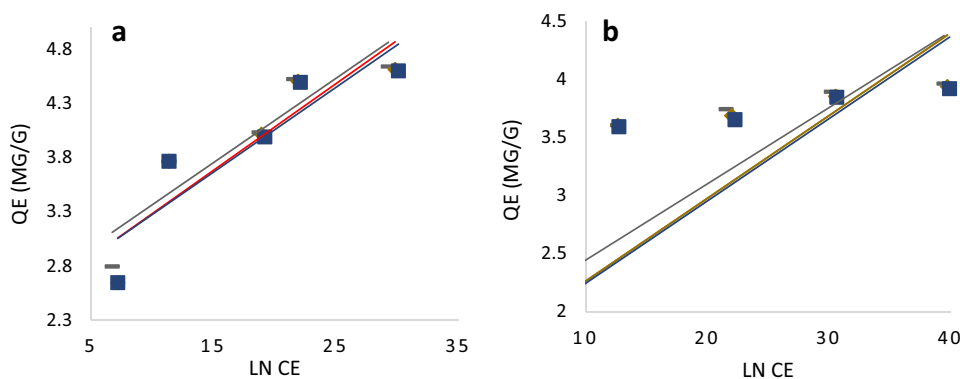


Fig. 9 Plot of q_e against $\ln C_e$ for the adsorption of phenol on **a** unmodified and **b** nanoparticle-modified AC



for the study in terms of energy cost. The ranges of the R^2 for both the NCAMSS (0.8159–0.8642) and the UCAMSS (0.4565–0.5321) activated carbons decreased with increasing contact time (Table 2) (Veli and Alyuz 2007).

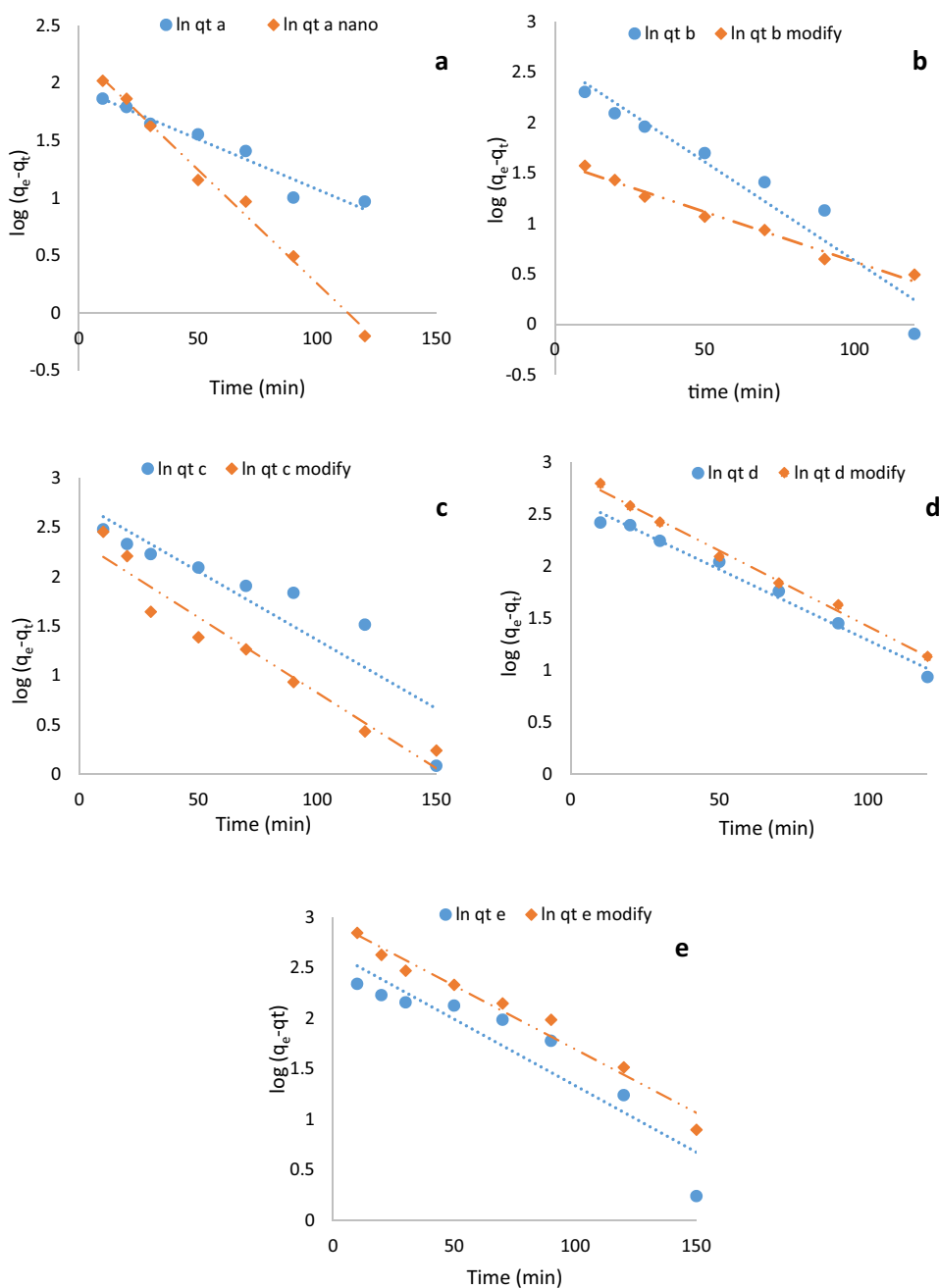
The R^2 values obtained from the Temkin isotherm were higher than the R^2 obtained for Langmuir Isotherm, yet they are lower than those obtained for Freundlich isotherm, and thus, the adsorption study fit best to Freundlich isotherms. The order of suitability of the isotherm models is Freundlich > Temkin > Langmuir. This suggested that the NCAMSS and UCAMSS adsorbents are characterised

by multilayer surface properties (Das et al. 2014; Ahsaine et al. 2018).

Kinetics Studies

The kinetic adsorption data can be processed to understand the dynamics of the adsorption reactions in terms of the order of the rate constant. The kinetic data were analysed using three different kinetic models: pseudo-first order, pseudo-second order, and Elovich equation. The plots of $\log(q_e - q_t)$ versus t (Fig. 10a–e) gave straight lines with values of k_1 and q_{cal} , evaluated from the slopes ($-k_1$) and intercepts

Fig. 10 Plot of $\log q_e - q_t$ against time for the adsorption process on modified and unmodified AC at initial concentration of **a** 50 mg/l, **b** 100 mg/l, **c** 150 mg/l, **d** 200 mg/l, and **e** 250 mg/l



($\ln q_e$) of the plots, respectively (Table 4). The plot of the concentration (50–250 mg/l) showed high relatively high R^2 (> 0.8) for both the UCAMSS and NCAMSS. The R^2 of the PFO for the NCAMSS and UCAMSS were in the ranges 0.8661–0.9925 and 0.8260–0.9942, respectively.

The values of k and q_e for the pseudo-second-order model were calculated from the intercepts ($1/kq_e^2$) and slopes ($1/q_e$) of the plots of t/q_t vs. t (Fig. 11a–e). The R^2 values of 0.6032–0.7505 and 0.4846–0.6032 obtained for NCAMSS and UCAMSS are lower than those obtained for PFO (Table 4) are. There is a wide difference between the calculated (q_{cal}) and experimental (q_{exp}) adsorption capacity under the evaluation of PSO, thus, suggesting its inappropriateness to describe the kinetic study of phenol onto the NCAMSS and UCAMSS (Gupta and Abdul Rafe 2013; Ahsaine et al. 2018). The comparison between the types of kinetics exhibited by other adsorbent–adsorbate relationship with this study is shown in Table 5. Adsorption of phenol on some materials displayed PSO, but the PFO reported in this study is well related to the kinetic order (PFO) reported by Gupta and Abdul Rafe (2013), which involved the application of Mango peel for the removal of phenol from wastewater.

The plot of q_t against $\ln t$ (Fig. 12a–e) provides a linear relationship where α and β were determined from the slope and intercept of the plot, respectively. The α (initial sorption rates) obtained for the NCAMSS and UCAMSS were in the ranges 0.0771–5.4380 mg/g min and 0.0384–3.8431 mg/g min, respectively. The values obtained for β , which are related to the extent of surface coverage and activated energy, were 1.654–5.5113 and 2.2608–4.176 g/mg, respectively. The evaluated Elovich parameters (Table 5) indicates that R^2 values obtained from Elovich equation were in the ranges of 0.9567–0.9929 and 0.8842–0.9786, for the NCAMSS and UCAMSS at the different initial phenol concentrations investigated (Table 6). This high R^2 values suggested that the adsorption process

display traced of chemisorption process (Elkady et al. 2011); however, higher R^2 values obtained for the first order suggested that the phenol adsorption was more influenced by a physisorption process (Rincon-Silva et al. 2016). The order of fitness/suitability of the models are pseudo-first order $>$ Elovich $>$ pseudo-second order.

Adsorption Mechanism

Weber and Morris intra-particle diffusion resistance model was used to determine the influence or identify the adsorption mechanism, and predicting the rate-controlling step in the adsorption of phenol onto the adsorbents produced (Weber and Morris 1963; Al-Othman et al. 2012). The values of K_i were calculated from slopes of the plots of q_t vs. $t^{0.5}$ (Fig. 13a–e) and the linear plot did not pass through the origin. The plots of intra-particle model equation for the UCAMSS and NCAMSS at different initial concentrations (50–250 mg/l) presented a multilinearity (Ramachandran et al. 2011). Three stages of diffusion was deduced from the plots. The first portion, which is steeper, can be classified as external surface, and the second portion, which is gradual, can be classified as rate controlled while the third portion, which is slow region, can be classified as equilibrium (Ramachandran et al. 2011). This indicated that the intra-particle diffusion was not only the rate-controlling step and boundary layer diffusion (Cheung et al. 2007; Kushwaha et al. 2014). The value of 'C' increased from –1.3078 to 16.138 and 1.0741 to 19.574 for UCAMSS and NCAMSS as the initial concentration increased for 50–250 mg/l. The C values obtained for the NCAMSS were higher than those obtained for the UCAMSS were correspondingly. K_i values also follow the similar trends except in a few cases, though K_i is always influenced by concentration driving force which is experienced by increased in adsorbate concentration (Ozer and Dursun 2007; Abdelwahab and Amin 2013).

Table 4 Kinetic parameters and correlation coefficients (R^2) obtained for the unmodified and modified models

Conc. (mg/l)	q_e (exp)	Pseudo-first order			Pseudo-second order			Elovich		
		q_e (cal)	K_1	R^2	q_e (cal)	K_1	R^2	α	β	R^2
Unmodified										
50	7.1818	7.0203	0.0087	0.9925	0.5346	–0.0484	0.7139	0.0384	2.2608	0.9239
100	11.3636	13.3151	0.0196	0.9799	0.2326	–0.1017	0.631	0.0404	3.4282	0.9786
150	19.1818	15.5491	0.0139	0.9451	0.3316	–0.0633	0.6315	0.1029	4.0501	0.9253
200	22.0909	14.2335	0.0137	0.9857	0.2491	–0.0827	0.6032	0.2029	4.1769	0.9544
250	30.0909	14.1427	0.0132	0.8661	0.9183	–0.0285	0.7505	3.8431	3.617	0.8842
Modified										
50	9.5455	9.3643	0.0198	0.9493	0.2151	–0.1151	0.7101	0.0771	2.61	0.9831
100	12.7273	4.9948	0.0099	0.9318	0.1200	–0.1900	0.5812	5.4380	1.654	0.9576
150	22.2727	10.5066	0.0153	0.826	0.3689	–0.0597	0.6837	0.7529	3.540	0.9567
200	30.6364	17.8267	0.0146	0.9942	0.1394	–0.1383	0.4846	0.2218	5.5113	0.9929
250	39.9091	19.1002	0.0126	0.9708	0.9183	–0.0175	0.5255	0.8848	5.5113	0.9723

Fig. 11 Plot of $\log t/q_i$ against time for the adsorption process on both modified and unmodified AC at initial concentration of **a** 50 mg/l, **b** 100 mg/l, **c** 150 mg/l, **d** 200 mg/l, and **e** 250 mg/l

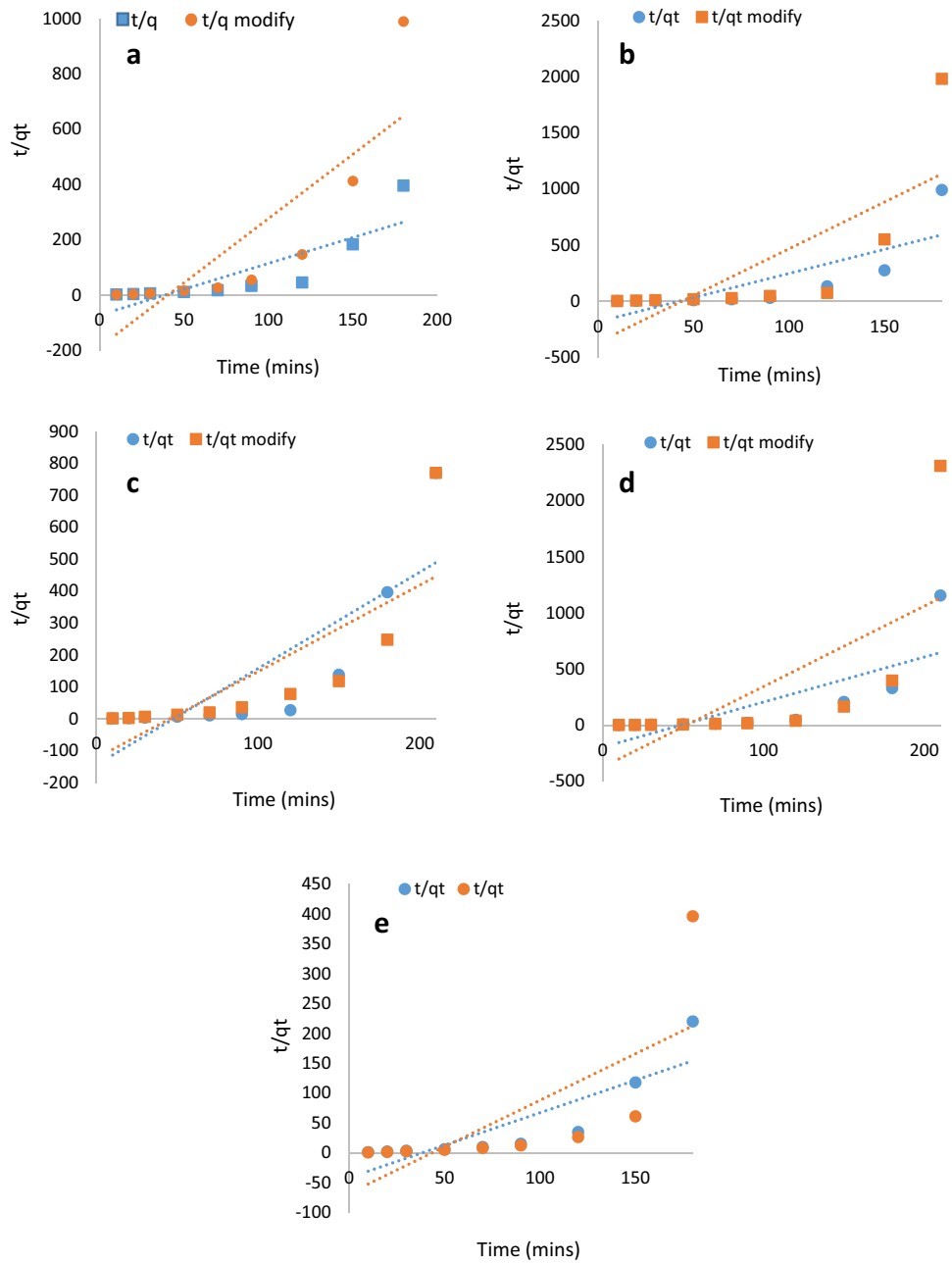


Table 5 Comparison between the types of kinetics exhibited by different adsorbent–adsorbate relationship

Adsorbent	Adsorbate	q_e (mg/g)	K_i	Kinetic	References
Mango peel	Phenol	17.534	0.3928	PFO	Gupta and Abdul Rafe (2013)
Mango kernel	Chromium (VI)	17.534	0.3928	PSO	Rai et al. (2016)
Coconut coir activated carbon	Phenol	588.24	0.00016	PSO	Ashanenduet al. (2018)
Modified Rhassoul (clay)	Phenol	13.24	0.007	PSO	Hamdaoui et al. (2018)
Organically modified manganite	Phenol	47.11	0.00045	PSO	Ge et al. (2019)
Unmodified mango seed shell AC	Phenol	7.0203–14.1427	0.0087–0.0132	PFO	This study
Nano-modified mango seed shell AC	Phenol	9.3643–19.1002	0.0126–0.0198	PFO	This study

PFO pseudo-first order, PSO pseudo-first order

Fig. 12 Plot of q_e against t for the adsorption process on both modified and unmodified AC at initial concentration of **a** 50 mg/l, **b** 100 mg/l, **c** 150 mg/l, **d** 200 mg/l, and **e** 250 mg/l

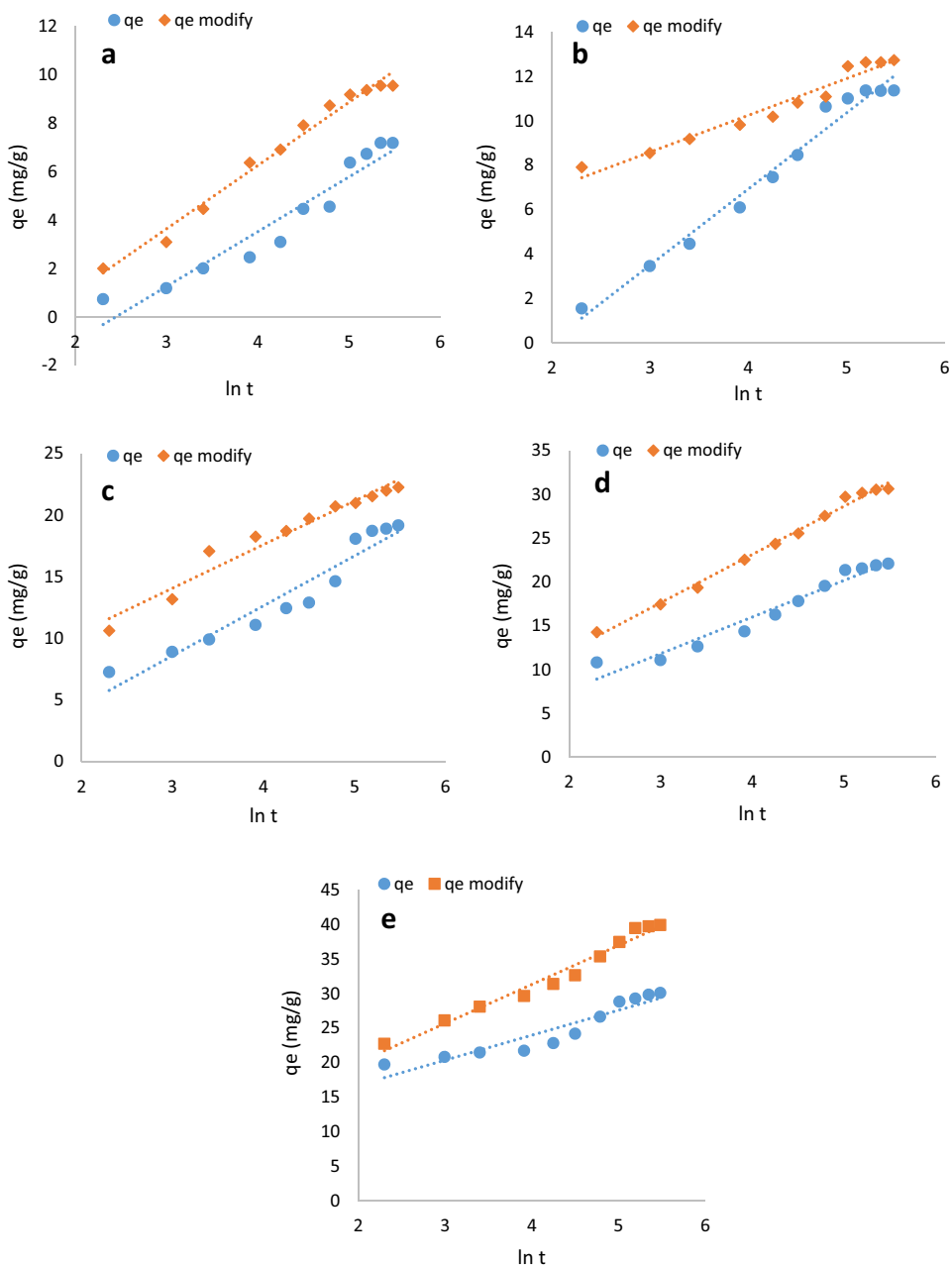
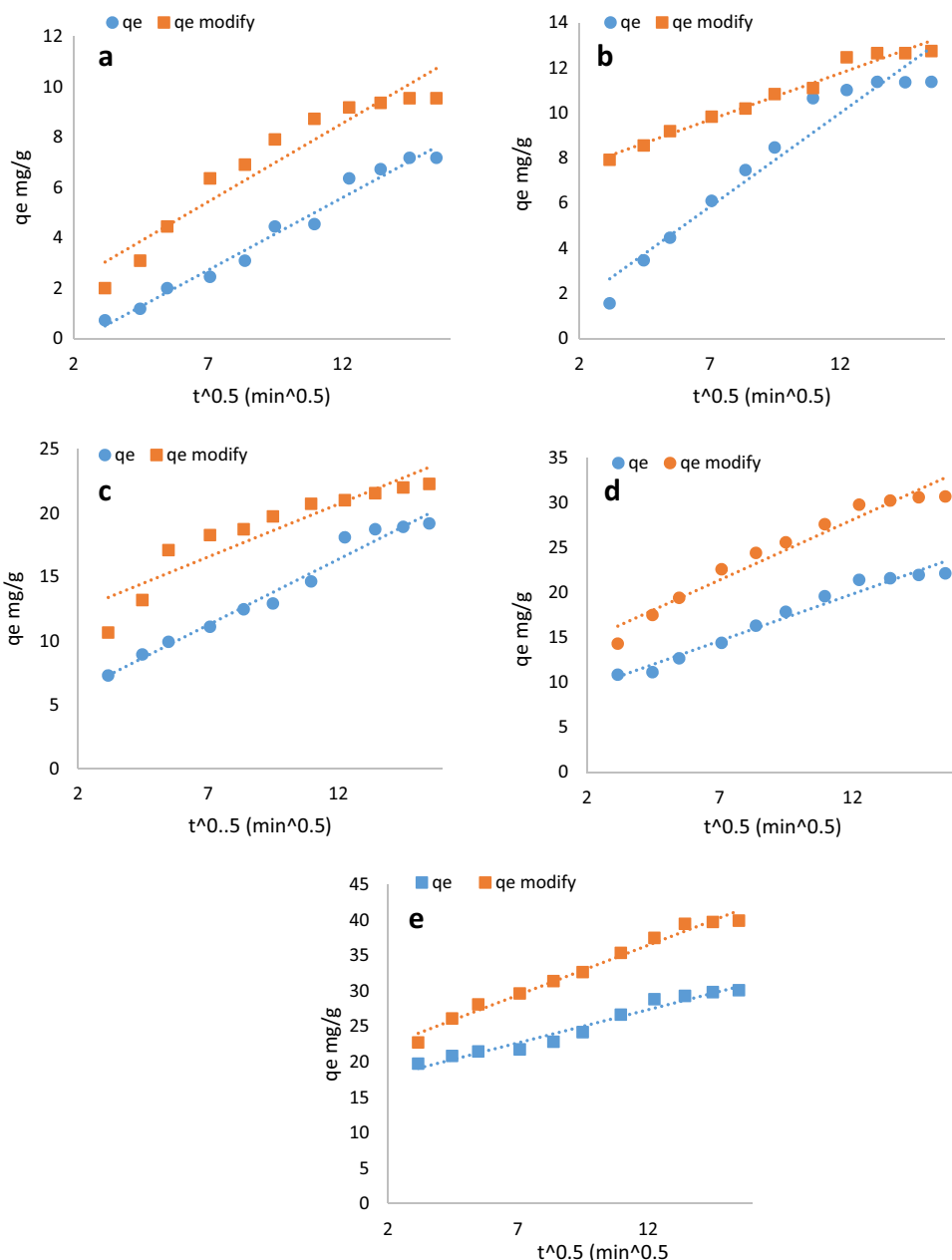


Table 6 Parameters for the intra-particle diffusion model

Conc. (mg/l)	Unmodified adsorbent			Nano-modified adsorbent		
	K_i	C	R^2	K_i	C	R^2
50	0.5762	-1.3078	0.9776	0.6238	1.0741	0.9148
100	0.8325	0.0044	0.9401	0.4131	6.7978	0.9729
150	1.0295	4.0337	0.9738	0.8281	10.775	0.8528
200	1.0429	7.3022	0.9693	1.3385	12.011	0.9539
250	0.9351	16.138	0.9625	1.4062	19.574	0.9822

Fig. 13 Plot of q_e against $t^{0.5}$ for the adsorption process on both modified and unmodified AC at initial concentration of **a** 50 mg/l, **b** 100 mg/l, **c** 150 mg/l, **d** 200 mg/l, and **e** 250 mg/l



Thermodynamic Studies

The thermodynamic parameters such as the standard enthalpy (ΔH°), standard free energy (ΔG°), and standard entropy (ΔS°) (Table 7) were evaluated from plot of $\ln K_d$ against $1/T$ (Vant Hoff’s plot) (Fig. 14a, b), to characterize the influence of temperature on transfer of solute from the solution onto solid–liquid interface (Bello et al. 2014). The ΔG° are negative except for 318 K and 333 K at 10 min for the UCAMSS and NCAMSS (Table 7). The ΔG° of the NCAMSS were higher than the UCAMSS and this indicated that adsorption process is spontaneous and feasible except for the ones at 318 K and 333 K, respectively. The decrease

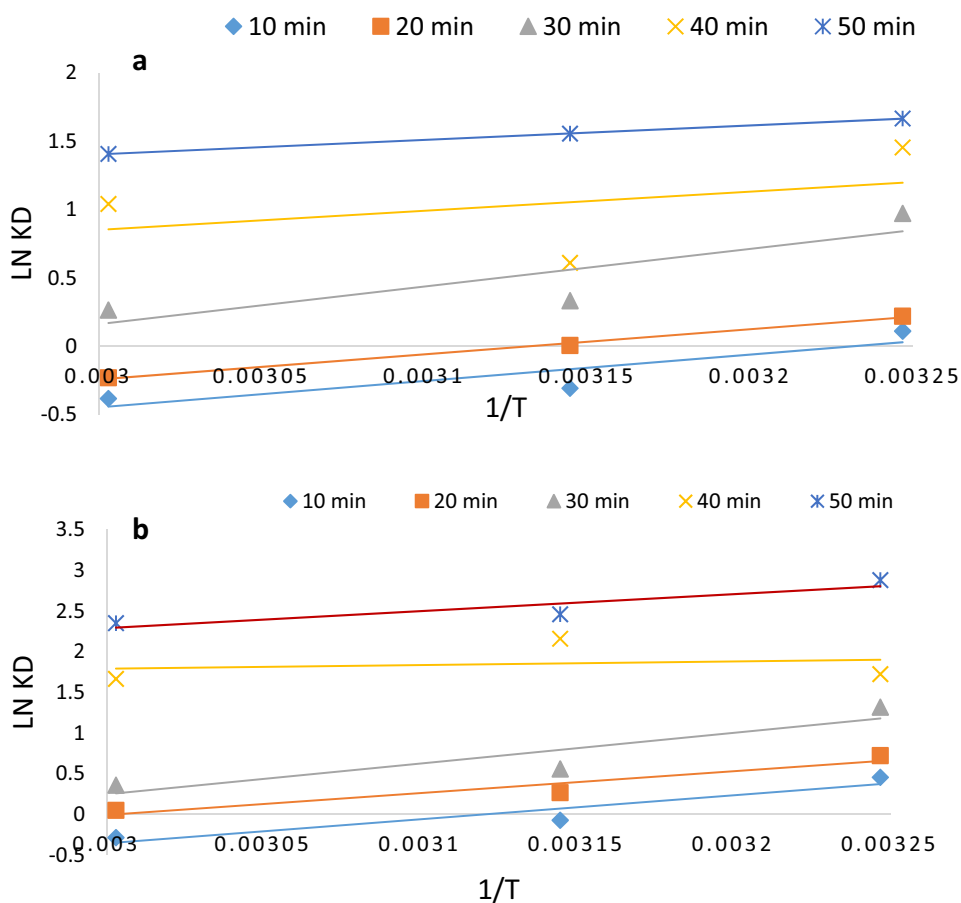
in negative value of ΔG° as the temperature increase indicated that adsorption decrease with rise in temperature. This change in ΔG° value may be due to the increase in degree of freedom, which might enhance desorption rather than adsorption at high temperatures (Rani and Sud 2015). Generally, the range of free energy values (ΔG°) for physisorption is between -20 and 0 kJ/mol, while chemisorption is between -80 and -400 kJ/mol. The value of the ΔG° fell within the range of 0 to -20 kJ/mol for the adsorption process on the UCAMSS and NCAMSS (Rani and Sud 2015).

The ΔH° values gotten were negative which varied from -8.8212 to -22.8643 kJ/mol for the UCAMSS and -3.694 to -31.402 kJ/mol for NCAMSS. This showed

Table 7 Thermodynamic parameters for the adsorption of phenol onto unmodified and nanoparticle-modified activated carbon

Time (min)	Temperature (K)	Unmodified activated carbon			Nanoparticle-modified activated carbon		
		ΔG (KJ/mol)	ΔH (KJ/mol)	ΔS (KJ/mol K)	ΔG (KJ/mol)	ΔH (KJ/mol)	ΔS (KJ/mol)
10	308	-0.285			-1.1649		
	318	0.8106	-16.035	-0.0518	0.1959	-24.521	-0.0765
	333	1.0564			0.7965		
20	308	-0.5633			-1.8483		
	318	-0.0180	-15.276	-0.0478	-0.7003	-22.339	-0.0671
	333	0.6382			-0.1332		
30	308	-2.4887			-3.3715		
	318	-0.8831	-22.864	-0.0672	-1.4718	-31.402	-0.0922
	333	-0.7333			-0.9899		
40	308	-3.7247			-4.4166		
	318	-1.6127	-11.635	-0.0278	-5.7094	-3.694	0.0038
	333	-2.8833			-4.6116		
50	308	-4.2654			-7.3776		
	318	-4.1129	-8.8212	-0.0148	-6.5078	-17.344	-0.0330
	333	-3.8951			-6.5099		

Fig. 14 a Van't Hoff's plot of $\ln K_d$ against $1/T$ for the adsorption of phenol onto unmodified AC. **b** Van't Hoff's plot of $\ln K_d$ against $1/T$ for the adsorption of phenol onto nanoparticle-modified AC



that the adsorption process was spontaneous, exothermic, and likely physisorption.. The small negative values of ΔS° (-0.0148 to -0.0672 kJ/mol K) UCAMSS and (-0.0330 to

0.0922 kJ/mol) NCAMSS suggested that there was decrease in the degree of randomness on solid/solute interface during the adsorption (Rani and Sud 2015). However, at 40 min for

Table 8 List of studies showing ΔG° , ΔH° , and ΔS° of the adsorption of phenol by activated carbon at different temperatures

Adsorbent	ΔG° (KJ/mol)	ΔH° (KJ/mol)	ΔS° (KJ/mol)	References
Luffa cylindrical fibres	– 1.8665	– 32.7	– 0.1265	Abdelwahab and Amin (2013)
Avocado kernel seed-activated carbon	– 13.695	– 212.400	– 0.6488	Dejene et al. (2016)
Graphene oxide	– 0.51	– 3.76	– 10.92	Wang et al. (2018)
Pineapple bark	– 3.86624	– 22.44	– 51.68	Fegousse et al. (2019)
Mango seed shell-activated carbon	– 4.2654	– 8.8212	– 0.0148	This study
Nanoparticle-modified activated carbon	– 7.3776	– 17.3438	– 0.0330	This study

the adsorption of phenol on NCAMSS, the ΔS° was positive. The comparison of the values of the parameters gotten from this study to other studies in which activated carbon removed phenol from wastewater using different adsorbent can be found in Table 8. All the values of ΔH° , ΔG° , and ΔS° reported in the previous and present study are negative (Table 8). The ΔS° obtained in this study were higher than those reported and this suggests that the degree of spontaneity of phenol adsorption onto the UCAMSS and NCAMSS is higher than some materials earlier reported for phenol adsorption.

Conclusion

The potential of Mango seed shell activated with BaCl_2 and further modified with silver–gold-based nanoparticles biosynthesized from *Cola nitida* has been studied for effective removal of phenol from synthetic wastewater. The FTIR characterisation of the modified and unmodified mango seed shell ACs showed the presence of additional functional groups on the surface of the modified ACs. The nanoparticle-modified activated carbon has the higher percentage removal compared to the unmodified activated carbon. The equilibrium data fitted well to the Freundlich isotherm model for the adsorption study, while the kinetic of the adsorption fitted best to the pseudo-first-order model. The intra-particle diffusion model showed that the rate-controlling step is influenced by pore diffusion and that boundary layer diffusion. The adsorption process is heterogeneous, exothermic, spontaneous, and decreased randomness on solid/solute interface. It can be deduced that mango seed shell is a good precursor in the production of activated due to its high yield and good adsorption capacity, and the modification of the activated carbon with nanoparticles increases the rate of adsorption.

References

Abdelwahab O, Amin N (2013) Adsorption of phenol from aqueous solutions by *Luffa cylindrica* fibers: kinetics, isotherm and thermodynamic studies. *Egypt J Aquat Res* 39:215–223

- Acosta C, López P, Paniagua G, Garcinuño R, Fernández H (2018) Evaluation of total phenol pollution in water of San Martin Canal from Santiago del Estero, Argentina. *J Environ Pollut* 236:265–272
- Ahsaine HA, Zbair M, Anfar Z (2018) Cationic dyes adsorption onto high surface area ‘almond shell’ activated carbon: kinetics, equilibrium isotherms and surface statistical modeling. *Mater Today Chem* 8:121–132
- Akpen G, Aho I, Mamwan M (2016) Removal of colour from textile wastewater by mango seed endocarp activated carbon. *Int J Sci Technol* 6(4):756–762
- Alabi O, Alade AO, Afolabi TJ (2019) Process optimization of adsorption of Cr(VI) on adsorbent prepared from *Bauhinia rufescens* pod by Box–Behnken design. *Sep Sci Technol*. <https://doi.org/10.1080/01496395.2019.1577436>
- Alencar WS, Acayanka E, Lima EC, Royer B, de Souza FE, Lameira J, Alves CN (2012) Application of *Mangifera indica* (mango) seeds as a biosorbent for removal of Victazol Orange 3R dye from aqueous solution and study of the biosorption mechanism. *Chem Eng J* 209:577–588
- Allen SJ, Whitten L, McKay G (2008) The production and characterisation of activated carbons: a review. *Dev Chem Eng Miner Process* 6(5):231–261
- Al-Othman ZA, Ali R, Naushad M (2012) Hexavalent chromium removal from aqueous medium by activated carbon prepared from peanut shell: adsorption kinetics, equilibrium and thermodynamic studies. *Chem Eng J* 184:238–247
- Al-Qodah Z, Shawabkah R (2009) Production and characterization of granular activated carbon from granular sludge. *Braz J Chem Eng* 26(1):127–136
- Amri N, Zakaria R, Abu Bakar M (2009) Adsorption of phenol using adsorbent from waste tyres. *Pertanika J Sci Technol* 17:371–380
- Ashanendu M, Paramartha M, Sudip K (2018) Removal of phenol from aqueous solution using activated carbon from coconut coir. *IOSR J Eng (IOSRJEN)* 8(12):41–55
- Bello O, Bello O, Lateef I (2014) Adsorption characteristics of mango leaf (*Mangifera indica*) as adsorbent for malachite green dye removal from aqueous solution. *Covenant J Phys Life Sci* 2:1–13
- Bouchelta C, Medjram MS, Bertrand O, Bellat J-P (2008) Preparation and characterization of activated carbon from date stones by physical activation with steam. *J Anal Appl Pyrolysis* 82:70–77
- Bruce RM, Santodonato J, Neal MW (1987) Summary review of the health effects associated with phenol. *Toxicol Ind Health* 3:535–568
- Bulgariu L, Bulgariu D, Macoveanu M (2011) Adsorptive performances of alkaline treated peat for heavy metal removal. *Sep Sci Technol* 46:1023–1033
- Bullut Y, Tez Z (2007) Adsorption studies on ground shells of hazelnut and almond. *J Hazard Mater* 149:35–41
- Cheung W, Szeto Y, McKay G (2007) Intraparticle diffusion processes during acid dye adsorption onto chitosan. *Bioresour Technol* 98:2897–2904

- Das B, Mondal NK, Bhaumik R, Ray P (2014) Insight into adsorption equilibrium, kinetics and thermodynamics of lead onto alluvial soil. *Int J Environ Sci Technol* 11:1101–1114
- Davila-Jimenez MM, Elizalde-Gonzalez MP, Hernandez-Montoya V (2009) Performance of mango seed adsorbents in the adsorption of anthraquinone and azo acid dyes in single and binary aqueous solutions. *Bioresour Technol* 100:6199–6206
- Dejene K, Siraj K, Kitte S (2016) Kinetic and thermodynamic study of phenol removal from water using activated carbon synthesized from Avocado kernel seed. *Int Lett Nat Sci* 54:42–57
- Dieguez-Santana K, Villegas-Aguilar P, Le-Thi-Thu H, Castillo-Garit J, Casañola-Martin GM (2016) Prediction of acute toxicity of phenol derivatives using multiple linear regression approach for *Tetrahymena pyriformis* contaminant identification in a median-size database. *Chemosphere* 165:434–441
- Dixon RA, Paiva NL (1995) Stress-induced phenylpropanoid metabolism. *Plant Cell* 7:1085
- Ejikeme PC, Ebere MO, Gloria N (2014) Equilibrium, kinetics and thermodynamic studies on basic dyes adsorption using composite activated carbon. *Int J Tech Res Appl* 2:96–103
- Elkady MF, Ibrahim AM, Abd El-Latif MM (2011) Assessment of the adsorption kinetics, equilibrium and thermodynamic for the potential removal of reactive red dye using eggshell biocomposite beads. *Desalination* 278:412–423
- Fegousse A, El Gaidoumi A, Miyah Y, El Mountassir R, Lahrichi A (2019) Pineapple bark performance in dyes adsorption: optimization by the central composite design. *J Chem*. <https://doi.org/10.1155/2019/3017163>
- Freundlich HMF (1906) Over the adsorption in solution. *J Phys Chem* 57:385–471
- Ge M, Wang X, Du M, Liang G, Hu G, Alam JSM (2019) Adsorption analyses of phenol from aqueous solutions using magadiite modified with organo-functional groups: kinetic and equilibrium studies. *Materials* 12:96. <https://doi.org/10.3390/ma12010096>
- Gumus R, Okpeku I (2015) Production of activated carbon and characterization from snail shell waste (*Helix pomatia*). *Adv Chem Eng Sci* 5:51–61
- Gupta A, Abdu Rafe M (2013) Removal of phenol from wastewater using mango peel. *Int J Eng Tech Res* 1:58–62
- Hamdaoui M, Hadri M, Bencheqroun Z, Draoui K, Nawdali M, Zaitan H, Barhoun A (2018) Improvement of phenol removal from aqueous medium by adsorption on organically functionalized Moroccan stevensite. *J Mater Environ Sci* 9(4):1119–1128
- Krishnaveni J, Renugadevi N (2012) Kinetic studies on biosorption of methyl violet dye using blue green algae. *Global J Sci Front Res Chem* 12(3):1–9
- Kulkarni SJ, Kaware DJP (2013) Review on research for removal of phenol from waste-water. *Int J Sci Res Publ* 3:1–4
- Kumar KV, Kumaran A (2005) Removal of methylene blue by mango seed kernel powder. *Biochem Eng J* 27:83–93
- Kushwaha A, Gupta N, Chattopadhyaya M (2014) Removal of cationic methylene blue and malachite green dyes from aqueous solution by waste materials of *Daucus carota*. *J Saud Chem Soc* 18:200–207
- Lekene NRB, Kouoh SPMA, Ndi NJ, Kouotou D, Belibi BPD, Ketcha MJ (2015) Kinetics and equilibrium studies of the adsorption of phenol and methylene blue onto cola nut shell based activated carbon. *Int J Cur Res Rev* 7(9):1–9
- Langmuir I (1916) The constitution and fundamental properties of solids and liquids. Part I. Solids. *J Am Chem Soc* 38:2221–2295
- Lateef A, Ojo S, Folarin B, Gueguim-Kana E, Beukes L (2016) Kolanut (*Cola nitida*) mediated synthesis of silver-gold alloy nanoparticles: antifungal, catalytic, larvicidal and thrombolytic applications. *J Cluster Sci* 15(5):1561–1577
- Lin L, Zhai S-R, Xiao Z-Y, Song Y, An QD, Song XW (2013) Dye adsorption of mesoporous activated carbons produced from NaOH-pretreated rice husks. *Bioresour Technol* 136:437–443
- Ma Y, Gao N, Chu W, Li C (2013) Removal of phenol by powdered activated carbon adsorption. *Front Environ Sci Eng* 7:158–165
- Meireles CS, Rodrigues-Filho GF, Jr MF, Cerqueira DA, Assunção RMN, Ribeiro P, Poletto MZ (2010) Characterization of asymmetric membranes of cellulose acetate from biomass: newspaper and mango seed. *Carbohydr Polym* 80:954–961
- Okeowo IO, Balogun EO, Alade AO, Afolabi TJ, Farombi AG (2017) Optimization of conditions for the production of activated carbon from mango seed shell using barium chloride as the activating agent. In: Paper presented at the 7th international biotechnology conference, exhibition and workshop. Covenant University, Ota
- Olajire A, Abidemi J, Lateef A, Benson N (2017) Adsorptive desulfurization of model oil by Ag nanoparticles-modified activated carbon prepared from brewer's spent grains. *J Environ Chem Eng* 5:147–159
- Olufemi BA, Otolorin F (2017) Comparative adsorption of crude oil using mango (*Mangifera indica*) shell and mango shell activated carbon. *Environ Eng Res* 22(4):384–392. <https://doi.org/10.4491/eer.2017.011>
- Ozer A, Dursun G (2007) Removal of methylene blue from aqueous solution by dehydrated wheat bran carbon. *J Hazard Mater* 146:262–269
- Rai M, Shahi G, Meena V, Meena R, Chakraborty S, Singh R et al (2016) Removal of hexavalent chromium Cr(VI) using activated carbon prepared from mango kernel activated with H₃PO₄. *Resour Efficient Technol* 2:63–70
- Ramachandran P, Vairamuthu R, Ponnusamy S (2011) Adsorption isotherms, kinetics, thermodynamics and desorption studies of reactive orange 16 on activated carbon derived from *Ananas comosus* (L.) Carbon. *ARPN J Eng Appl Sci* 6(11):15–26
- Rani S, Sud D (2015) Effect of temperature on adsorption-desorption behaviour of triazophos in Indian soils. *Plant Soil Environ* 61:36–42
- Rincon-Silva N, Moreno-Pirajan J, Giraldo L (2016) Equilibrium, kinetics and thermodynamics study of phenols adsorption onto activated carbon obtained from lignocellulosic material (*Eucalyptus globulus* labill seed). *Adsorption* 22:33–48
- Shirzad-Siboni M, Jafari S, Farrokhi M, Yang J (2013) Removal of phenol from aqueous solutions by activated red mud: equilibrium and kinetics studies. *Environ Eng Res* 18(4):247–252
- Simha P, Banwasi P, Mathew M, Ganesapillai M (2016) Adsorptive resource recovery from human urine: system design, parametric considerations and response surface optimization. *Proc Eng* 148:779–786
- Srivastava V, Swamy MM, Mall I, Prasad B, Mishra I (2006) Adsorptive removal of phenol by bagasse fly ash and activated carbon: equilibrium, kinetics and thermodynamics. *Colloids Surf* 272:89–104
- Tchounwou P, Yedjou C, Patlolla A, Sutton D (2014) Heavy metal toxicity and the environment. *Mol Clin Environ Toxicol* 101:133–164
- Tichapondwa S, Tshemese S, Mhike W (2018) Adsorption of phenol and chromium (VI) pollutants in wastewater using exfoliated graphite. *Chem Eng Trans* 70:847–852
- Tossou G, Ekou L, Ekou T (2019) Adsorption of phenol on carbon based on cactus and banana peel. *Aust J Basic Appl Sci* 13(1):64–70
- Varghese S, Vinod V, Anirudhan T (2004) Kinetics and equilibrium characterization of phenols adsorption onto a novel activated carbon in water treatment. *Indian J Chem Technol* 11:825–833
- Veli S, Alyuz B (2007) Adsorption of copper and zinc from aqueous solutions by using natural clay. *J Hazard Mater* 149:226–233

- Wallace J (1996) Phenol. In: Kirk–Othmer encyclopaedia of chemical technology, 4th edn. Wiley, New York, pp 592–602
- Wang X, Hu Y, Min J, Li S, Deng X, Yuan S et al (2018) Adsorption characteristics of phenolic compounds on graphene oxide and reduced graphene oxide: a batch experiment combined theory calculation. *Appl Sci* 8:1–13
- Williams PT, Reed AR (2003) Pre-formed activated carbon matting derived from the pyrolysis of biomass natural fibre textile waste. *J Anal Appl Pyrolysis* 70(2):563–577
- Weber WJ, Morris JC (1963) Kinetics of adsorption carbon from solutions. *J Sanit Eng Div* 89:31–60
- Zbair M, Bottlinger M, Brahmi R, Ainassaari A, Pirilä M, Drif A, Keiski RL, Ojala S, Bensite M (2017) Toward new benchmark adsorbents: preparation and characterization of activated carbon from argan nut shell for bisphenol A removal. *Environ Sci Pollut Res*. <https://doi.org/10.1007/s11356-017-0634-6>
- Zbair M, Ahsaine HA, Anfar Z (2018a) Porous carbon by microwave assisted pyrolysis: an effective and low-cost adsorbent for sulfamethoxazole adsorption and optimization using response surface methodology. *J Clean Prod*. <https://doi.org/10.1016/j.jclepro.2018.08.155>
- Zbair M, Bottlinger M, Ainassaari K, Ojala S, Stein O, Keiski RL, Bensitel M, Brahmi R (2018b) Hydrothermal carbonization of argan nut shell: functional mesoporous carbon with excellent performance in the adsorption of bisphenol A and diuron. *Waste Biomass Valoriz*. <https://doi.org/10.1007/s12649-018-00554-0>
- Zbair M, Anfar Z, Ahsaine HA, Khallok H (2019) Kinetics, equilibrium, statistical surface modeling and cost analysis of paraquat removal from aqueous solution using carbonated jujube seed. *RSC Adv* 9:1084–1094
- Zhang J (2013) Phenol removal from water with potassium permanganate modified granular activated carbon. *J Environ Prot* 4:411–417
- Zhong Y (2017) Analysis of congo red adsorption capability of the Mn-modified diatomite. *Chem Eng Trans* 62:25–30